Supporting Information

A "Ship in a Bottle" Strategy to Load a Hydrophilic Anticancer Drug in Porous Metal-Organic Frameworks Nanoparticles: Efficient Encapsulation, Matrix Stabilization, and Photodelivery

Maria Rosaria di Nunzio,[#a] Valentina Agostoni,[#b] Boiko Cohen,[a] Ruxandra Gref,[b]*

Abderrazzak Douhal[a]

# These authors contributed equally;

*Corresponding authors: Abderrazzak.douhal@uclm.es (A.D.) and ruxandra.gref@u-psud.fr (R.G.)

[#]Dedicated to Fatna Douhal died during the elaboration of this work.

[a] Departamento de Química Física, Facultad de Ciencias Ambientales y Bioquímica, and INAMOL, Universidad de Castilla-La Mancha, Avenida Carlos III, S/N, 45071 Toledo, Spain;

[b] UMR CNRS 8612, Faculty of Pharmacy, Paris-Sud University, 5 rue Jean Baptiste Clément, I-92290 Châtenay-Malabry (France).

Supplementary Text

Estimation of the Percentage of 1 Monomer (M) and Dimer (D) at a Given Concentration of the Drug

The reaction for the **1** dimerization is given by Equation S1:

$$M + M \Leftrightarrow D \tag{S1}$$

were M and D represent the monomer and the dimer of **1**, respectively. The following equations are true for the monomer-dimer equilibrium in solution at any **1** concentration (c_j):

$$c_j = c_{1j} + 2 \times c_{2j} \tag{S2}$$

$$K_d = \frac{c_{2j}}{c_{1j}^2} \tag{S3}$$

where c_{1j}, c_{2j}, and c_j are the concentrations of monomers, dimers and total **1** concentration in solution. K_d is the dimerization constant. Substitution of c_{2j} from Equation S3 in Equation S2 gives Equation S4:

$$c_j = c_{1j} + 2 \times K_d \times c_{1j}^2 \tag{S4}$$

Equation S4 allows the calculation of c_{1j} at a given concentration (c_j) of **1**. c_{2j} is then obtained from Equations S2 or S3.

Estimation of the Number of 1 Molecules Entrapped within LC and Cages Volume Occupancy at Each Drug Payload

Zeotype architecture MTN = $2[5^{12}] + [5^{12}.6^4]$
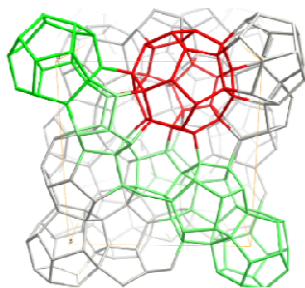
$[5^{12}]$ = small mesoporous cages (SC) delimited by 12 microporous pentagonal windows

$[5^{12}.6^4]$ = large mesoporous cages (LC) delimited by 12 microporous pentagonal windows and 4 microporous hexagonal windows

20: Iron trimers/SC

28: Iron trimers/LC

$$Fe(III)trimersLC\% = \frac{Fe(III)trimersLC}{Fe(III)trimersTotal}\% = 41.18\% \tag{S5}$$

Mw Fe(III) trimer = 669.45 g mol^{-1}

Mw **1** = 457.9 g mol^{-1}

The number of moles of **1** per mole of Fe(III) trimer at each payload is deduced from Equation S6:

$$N_0 = \frac{TPTmol}{Fe(III)mol} \tag{S6}$$

Starting from this ratio we calculated the number of **1** molecules (N1) interacting with 100 Fe(III) trimers (Equation S7):

$$N_1 = N_0 \times 100 \tag{S7}$$

Giving that only the LC are accessible to the drug, only the 41.18 % of the trimers are effectively available for the interaction. The number of **1** molecules (N2) interacting with each trimers within the LC is the following (Equation S8):

$$N2 = \frac{N1}{41.18} \tag{S8}$$

Considering that each LC contains 28 trimers. the number of **1** molecules/LC (N3)is the following (Equation S9):

$$N3 = N2_0 \times 28 \tag{S9}$$

The **1** volume (811 Å^3) has been evaluated by using ChemBio3D Ultra, while the volume of the big cages has been calculated by approximation with a sphere.

### *In Vitro* Activity of 1-Loaded MIL-100 NanoMOFs

Table S1. Tested concentrations of nanoparticles (µg/mL) and 1 (µM)

|	[MIL-100 nanoMOFs] (µg/mL) / ([**1**] , (µM))								
1	(0.01)	(0.02)	(0.1)	(0.2)	(1.2)	(6)	(18)	(36)	(72.3)
MIL-100(**1**)	0.01 (0.003)	0.1 (0.03)	0.5 (0.1)	1 (0.2)	5 (1.3)	25 (6)	75 (19.7)	150 (39.3)	300 (78.6)
MIL-100	0.01	0.1	0.5	1	5	25	75	150	300

1 Dimerization Process

The **1** dimerization process (Scheme S1) is well known. It is accompanied by an increase (from 6.5 to 7.1) and a decrease (from 10.7 to 10.3) in the pK$_a$ values of the 10-hydroxyl (OH) and 9-dimethylaminomethylene groups of the A-ring, respectively (Scheme 1 in the main text), when the concentration of the drug varies between 10^{-6} and 10^{-4} M (*2*). This further suggests that these groups are implicated in the dimer formation. Hence, the **1** molecules aggregate most probably through the instauration of an intermolecular H-bond with the N1 atom of the B-ring of a neighboring molecule. The retention exerted to the proton at the OH group by the intermolecular H-bond within the dimer accounts for the observed increase of its basicity. In addition, stacking interactions between the A-rings of both the monomers may contribute to stabilize the dimeric structure. Since the non-planarity of its molecular skeleton, the **1** dimer can exist in three probable forms, i.e., with both the E-rings of the monomers directed in opposite directions (out or into the dimer, Da and Db in Scheme S1,

respectively), or in to the same side (Dc in Scheme S1) (2).The **1** dimerization constant, K_d, has been determined to be $(4.0 \pm 0.7) \times 10^3 \ M^{-1}$.[1]
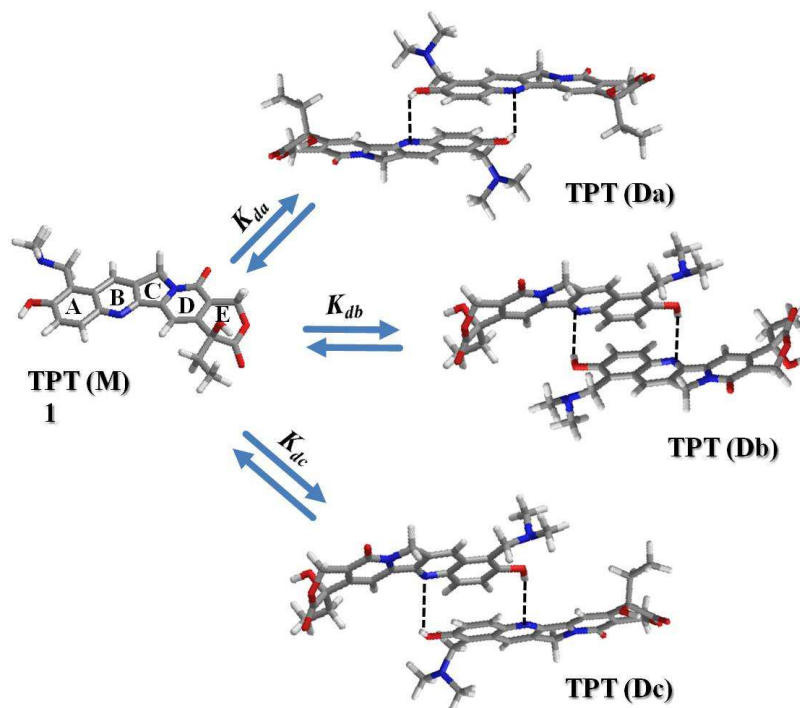
Scheme S1. Supposed equilibria between **1** in its monomeric (M) and dimeric (Da, Db, and Dc) forms.

The dimerization process was also observed by UV-visible spectroscopy as the spectra of **1** monomer (M) and dimer (D) exhibit typical signatures. Figure S1 shows the UV-visible absorption and emission (exciting at 371 nm) spectra of **1** in water (pH ~ 6.7) at concentrations $C_01 - C_04$.
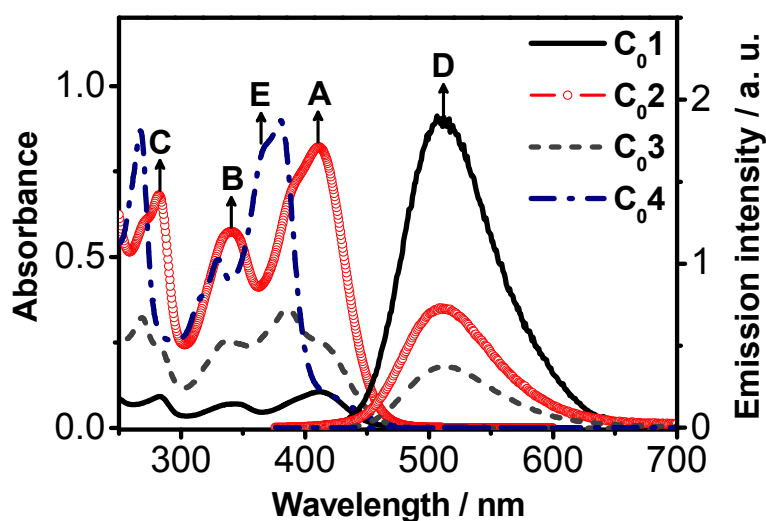

Figure S1. Absorption and emission (λ_{exc} = 380 nm) spectra of **1** in water (pH ~ 6.7) at different concentrations ($C_01 = 4.15 \times 10^{-6}$M; $C_02 = 4.15 \times 10^{-5}$M, $C_03 = 1.42 \times 10^{-4}$ M, and $C_04 = 4.15 \times 10^{-4}$M). The absorption spectra of **1** at concentrations C_03 and C_04 were collected using a 1 mm-path cell,

while those of emission were collected using a triangular cell. For $C_0 1$ and $C_0 2$, a 10 mm-path cell was used for both absorption and emission spectra. All the emission spectra are corrected for the absorption differences at the wavelength of excitation (380 nm). The absorption spectra of $C_0 3$ and $C_0 4$ should be multiplied by factor of 10. The arrows A, B, C, D, and E are just to guide the eyes.

In dilute water solution ($C_0 1$), the intensities of the absorption bands (412, 342, and 282 nm, A, B, and C in Figure S1) and emission (540 nm, D in Figure S1) have been previously assigned to Z (Scheme S1), which is the most abundant protolytic form of the drug in this concentration range.[2] A relative decrease in the absorption at 412 nm and concomitant increase of that in the 380-386 nm (E in Figure S1) region is observed when the concentration of **1** raises up to $C_0 4$. This effect is due to the reduction of the ground-state population of A when dimmers are formed. As a consequence, the salt bridge involving the 10- and 9-substituents in Z becomes weakened, thus increasing the acidity of the dimethylamino group. At high drug concentrations, the **1** enol and cation forms (λ_{abs} = 380 nm for **1** at concentration $C_0 4$) are the most abundant species that exist either as M or D. The radiative emission of **1** is strongly quenched in the presence of D (Figure S1), the intensity of the fluorescence spectrum waning by a factor of ~ 500 when going from $C_0 1$ to $C_0 4$. Similar observation have been reported for Rhodamine 6G, with a close structure, where the dominant mechanism of the fluorescence quenching in aqueous solutions has been ascribed to a long-range dipole-dipole energy transfer to the aggregates.[3]

Integrity of the NanoMOFs During Encapsulation

By XRPD it was assessed that the drug loading did not affect the nanoparticles supramolecular structure (Figure S2). Indeed, empty (green line) and **1**-loaded nanoMOF (blue line) containing a 10 wt% of drug showed overlapping spectra.
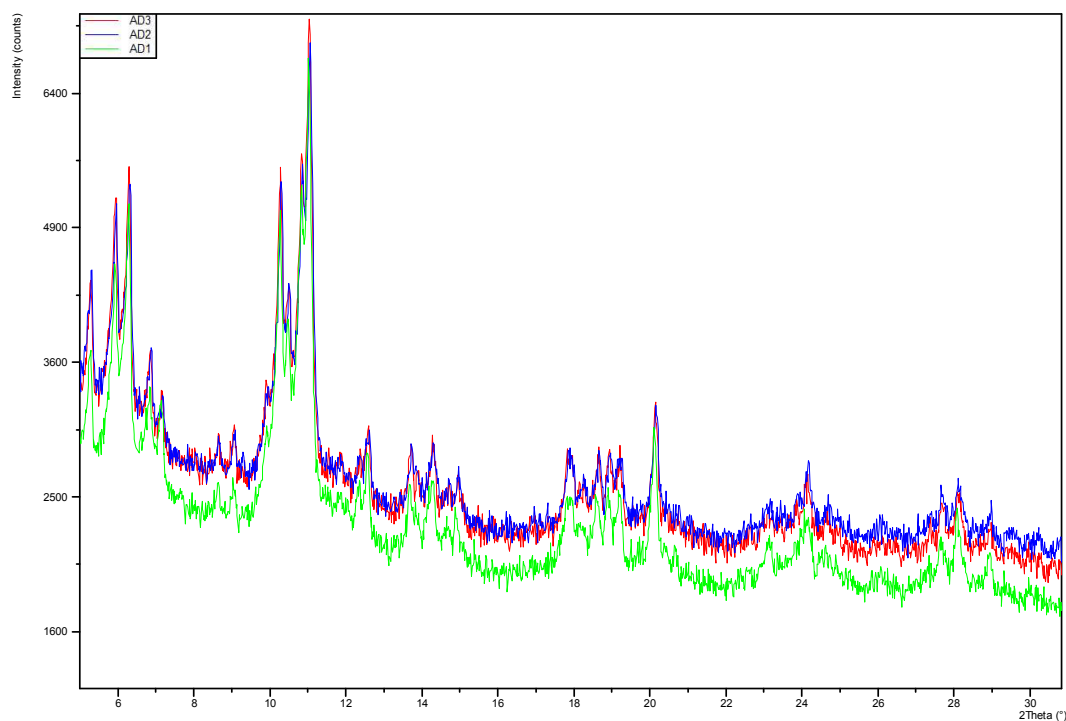

Figure S2. XRPD patterns of nanoMOF (green line), **1**-loaded nanoMOF before (blue line) and after two-photons irradiation (red line).

On the contrary, the Zeta potential gained more negative values (-15.6 ± 0.2 mV vs -32.5 ± 0.2 mV in empty MIL-100 nanoMOFs and **1**-loaded MIL-100 at maximal payload, respectively), suggesting the

presence of drug molecules adsorbed on the MIL-100s' surface. This provoked also a perceptible change of the colour of the **1**-loaded nanoMOFs, which passed from red (at low-medium payloads) to dark brown (only at the highest payload of 33 wt%). In conclusion, **1** loading did not affect the morphology or the size of the nanoMOFs.

Finally, by N_2 adsorption measurements, a marked decrease in the nanoparticles porous surface was observed after **1** loading (S_{BET} = 1444 vs 1054 m^2g^{-1} for nanoMOF and **1**-loaded nanoMOFs, respectively) suggesting an effective drug absorption within the nanoMOF porous core (Figure S3).
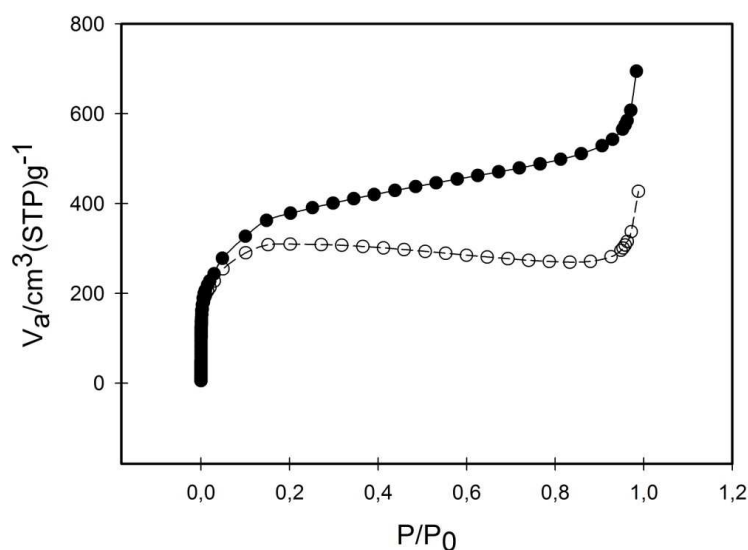
Figure S3. N_2 isotherms of MIL-100 nanoparticles before (black dots) and after **1** loading (white dots).

As reported in Figure S4A, at low drug concentration ($C_0$1), the entire amount of the drug was soaked out of the aqueous solution by the nanoMOFs, as it is evidenced from the efficient reduction of the fluorescence signal after incubation with the nanoparticles. When increasing the topotecan (TPT) concentration, the reduction of the fluorescence signal, defined as ratio of the emission intensity maxima of **1** (TPT) at 540 nm before (IC_0i) and after (IC_Si) 24 hours of impregnation, became less evident (Figure S4B).
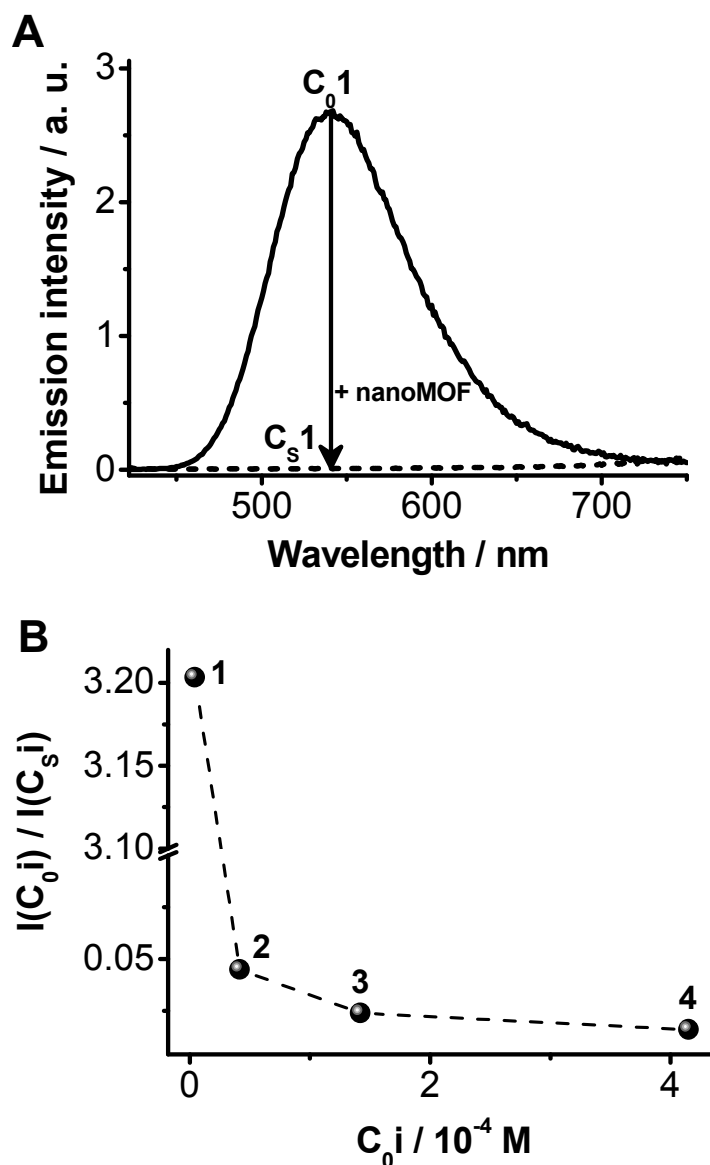
Figure S4. (A) Emission spectra (λ_{exc} = 411 nm) of **1** in water (pH ~ 6.7) with initial concentration $C_0 1$ = 4.15 × 10^{-6} M (solid line) and supernatant solution ($C_S 1$, dashed line) recovered by centrifugation (10 minutes at 10000 ×g) after 24 hours of impregnation of **1** $C_0 1$ with nanoMOFs. (B) Ratio of the emission intensity maxima (540 nm) of **1** before ($IC_0 i$) and after ($IC_S i$) 24 h of impregnation with nanoMOFs. The concentrations are $C_0 1 - C_0 4$. Except for $C_0 1$ and $C_S 1$, the solutions were diluted (up to 1:60, depending on the concentration) before the analysis.

Estimation of the Number of 1 Molecules Gathered *per* Large Cage and Large Cage's Volume Occupancy at Each Drug Payload

Calculations were performed according to the method described in materials and methods section.

Table S2. Number of 1 molecules entrapped within LC and cages volume occupancy at each drug payload achieved by single impregnation

| Payload	(1/trimers) ratio (N0)	(1/ trimers) % (N1)	1/trimer$_{LC}$ (N2)	1/ LC (N3)	LC occupancy (%)
0.14	0.0020	0.20	0.005	0.14	0.9
1.29	0.0189	1.89	0.046	1.28	8
4.24	0.0620	6.20	0.151	4.21	29
5.6	0.0819	8.19	0.199	5.57	36
33.04	0.4830	48.30	1.173	32.84	245

Table S3. Number of 1 molecules entrapped within LC and cages volume occupancy at each drug payload achieved by repetitive impregnations

payload	1/ LC (N3)	LC occupancy (%)
4.06	4	26
6.85	6.8	43
8.68	8.6	55
9.64	9.5	61
10.21	10.1	64
11.07	11	70
11.6	11.5	73

## *Steady-State Observations of 1-Loaded NanoMOFs in the Solid State. Dimerization within LC*

To study the state of aggregation of **1** in the nanoMOFs, steady state UV-visible diffuse reflectance spectra were recorded on dried particles. It should be noted that neither steady-state or time-resolved (using a 40 ps pulsed (20 MHz) diode laser centered at 371 or 433 nm) emission could be recorded most probably due to efficient quenching of the radiative processes due to the strong coordination of **1** with the nanoMOF matrix. Indeed, nanoMOFs coordination with various species (CO_2, amines, N-heterocyclic aromatics, carboxylic group) has been described.[4,5]
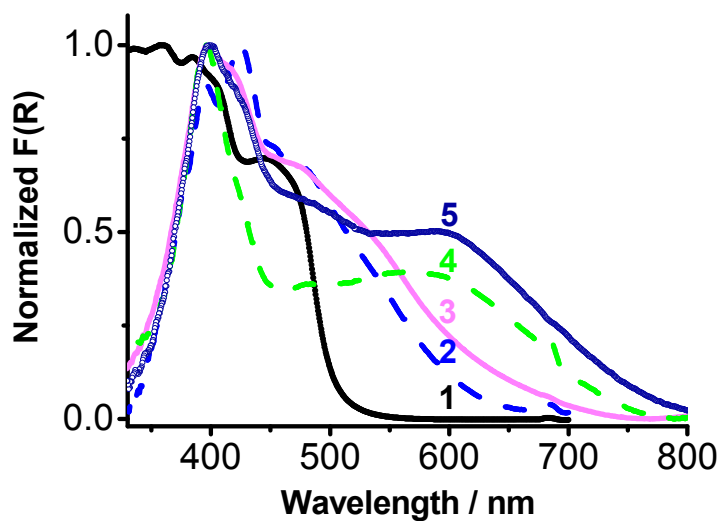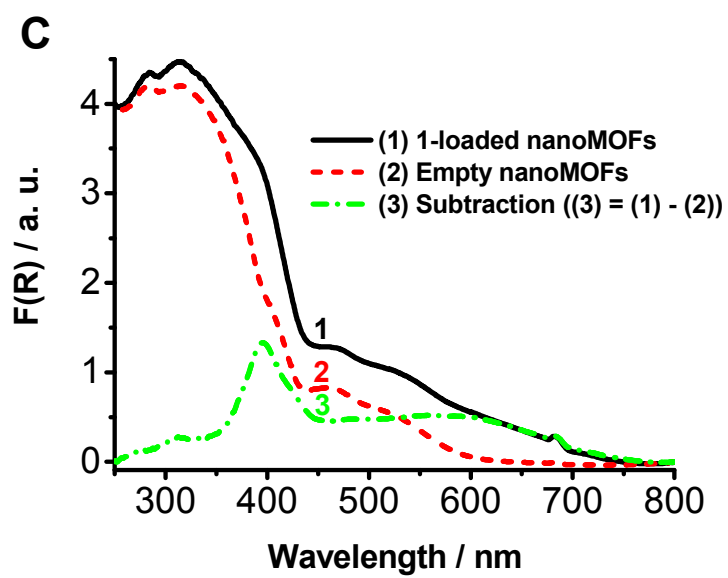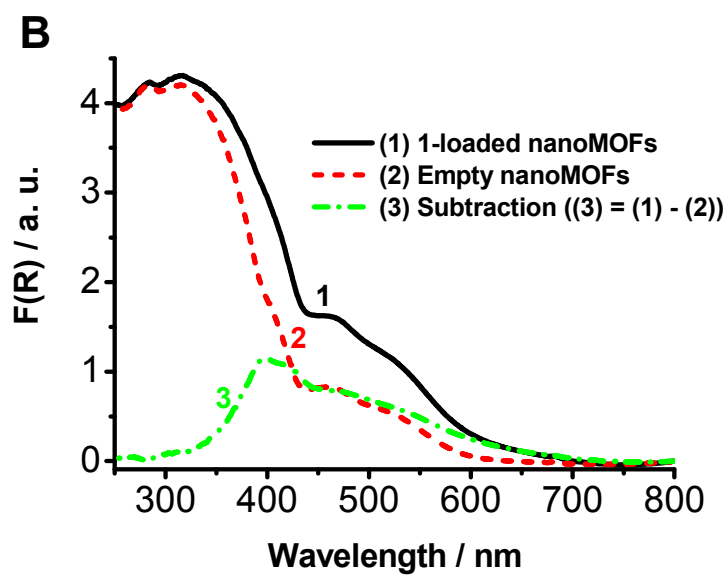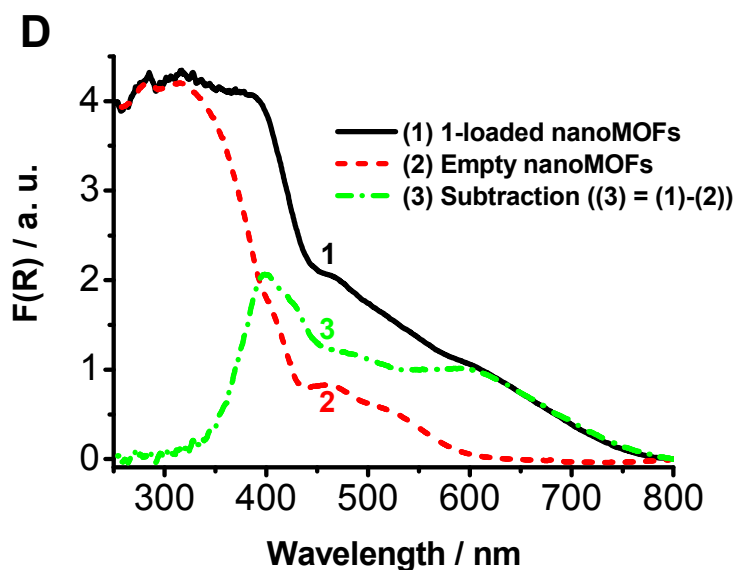
Figure S5. Normalized (to 1) diffuse reflectance (Kubelka-Munk units) values of **1** in the solid state free (1) and interacting with nanoMOFs at four representative payloads (0.14%, (2); 1.3%, (3); 5.6%, (4), and 33%, (5)). The spectra 2−5 were obtained after subtracting the contribution of the empty nanoMOFs (used as the reference, spectrum 1) to the total signal of the sample.

Determination of the UV-Visible Reflectance Spectra of 1-Loaded NanoMOFs in the Solid State
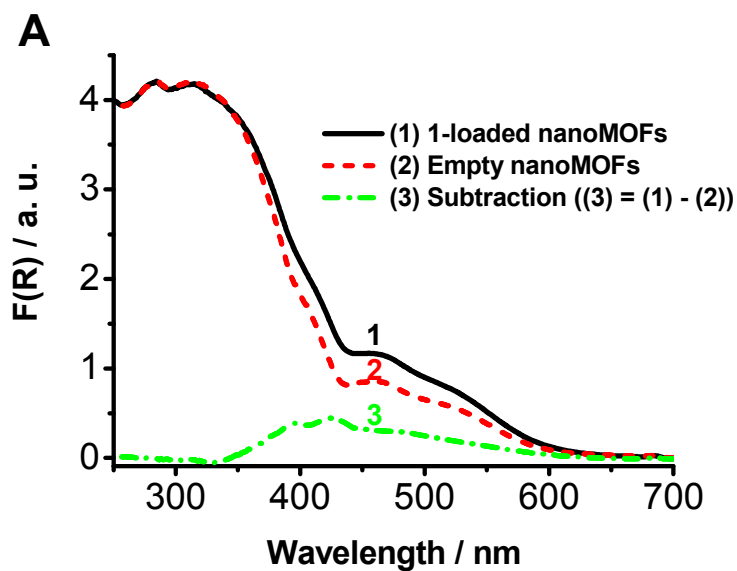
Figure S6. Diffuse reflectance (Kubelka-Munk units) values of **1**-loaded nanoMOFs in the solid state (3) at four representative payloads (0.14%, (A); 1.3%, (B); 5.6%, (C), and 33.1%, (D)). Spectrum 3 of each figure is obtained by subtracting the contribution of the empty nanoMOFs (2) to the total signal (1).

1-Loaded MIL-100 NanoMOF Degradation Over 25h of Incubation in Different Release Media

Table S4. Trimesate release from MIL-100 nanoMOF loaded with different 1 payloads and incubated 25h in different media with or without one- or two-photon excitation, as measured by HPLC

1 loading (wt%)	BTC release (%)			
	PBS	H_2O	H_2O (1 photon ex)	H_2O (2 photon ex)
0	N.D.	N.D.	N.D.	5.4
1.4	75.5	5.1	N.D.	N.D.
4	71.7	N.D.	N.D.	N.D.
12	6.9	4	N.D.	6.5
33	17.3	N.D.	6.2	8

N.D. = not determined.

Stability of the 1-Loaded NanoMOFs

The spectral features displayed by the highest **1**-loaded (33 wt%) nanoMOFs did not undergo any substantial spectral change after 15 days storage at 22°C under the dried form (Figure S10). This result is of high importance as it demonstrates a good shelf stability of the loaded nanoMOFs even after several days of storage. As a final consideration, the release capability of the 15 days-old **1**-loaded nanoMOFs after 15 days storage has been investigated and was still effective.
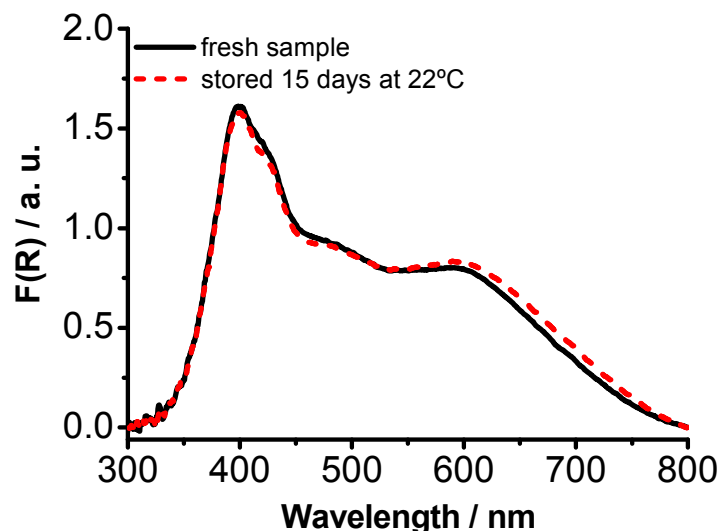
Figure S7. Diffuse reflectance (Kubelka-Munk units) values of **1**-loaded (payload = 33 wt%) nanoMOFs freshly prepared (black solid line) and after 15 days storage at 22ºC (red dashed line).

1-MIL-100 NanoMOFs Binding Isotherms Obtained by Isothermal Titration Calorimetry (ITC)

The interaction taking place between nanoMOFs and **1** was deeper characterized by isothermal titration calorimetry (ITC). An isothermal calorimeter (VP-ITC, MicroCal Inc., USA) was used to evaluate the interactions between MIL-100 nanoMOFs and **1**. In a typical experiment, aliquots of 10 µL of **1** (2.56 mM) aqueous solutions filled into 283 µL syringe were used to titrate a suspension of MIL-100 (1.9 mM; this concentrations is referred to the iron trimers defined by the previously calculated molecular formula)[1] into the calorimetric cell accurately thermostated at 25 °C. Intervals between injections were 300 s and agitation speed was 394 rpm. Background of titration consisted on injecting the **1** at the same concentration into deionized aqueous solution. The corresponding heat flow recorded as a function of time accounts for dilution effect.
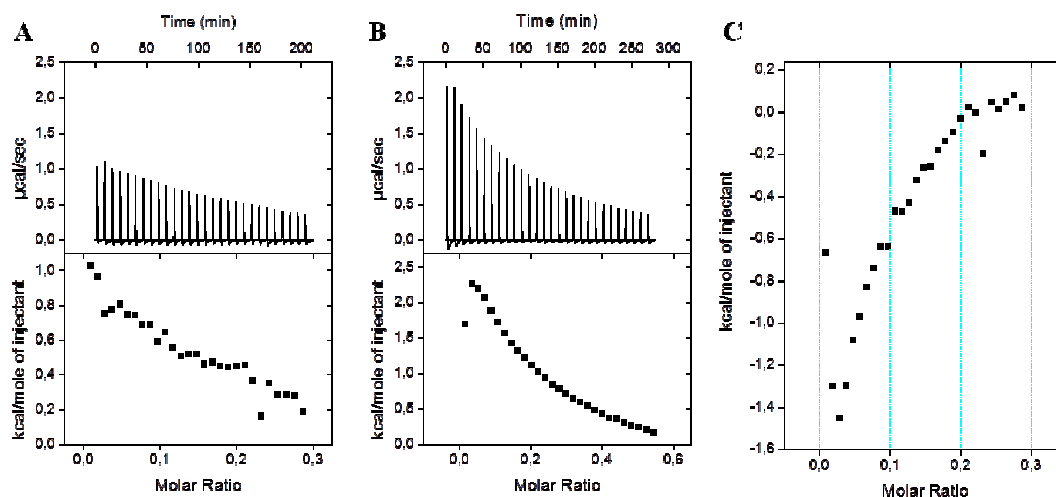
Figure S8. Thermograms obtained by titrating **1** (2.56 mM) into a nanoMOFs aqueous solution (1.9 mM) (A) or in water (B). **1**-nanoMOFs binding curve normalized for the drug's dilution in water (C).

1 dilution in water gave rise to important endothermic signal probably related to the dissociation of drug dimers. The thermograms achieved by titrating **1** into a nanoMOFs aqueous solution showed the same profile but less intense peaks. The **1**-nanoMOFs binding curve normalized for the drug dilution in water showed therefore a weak exothermic interplay between the drug and the nanoparticles.

Figure S9 reports the diffuse reflectance (A) and the emission intensity (λ_{exc} = 411 nm) (B) values of the nanoMOFs in PBS. Insets of Figure S11 show the variation of the (A) diffuse reflectance and (B) emission intensity values of the nanoparticles observed at 389 and 540 nm, in that order.
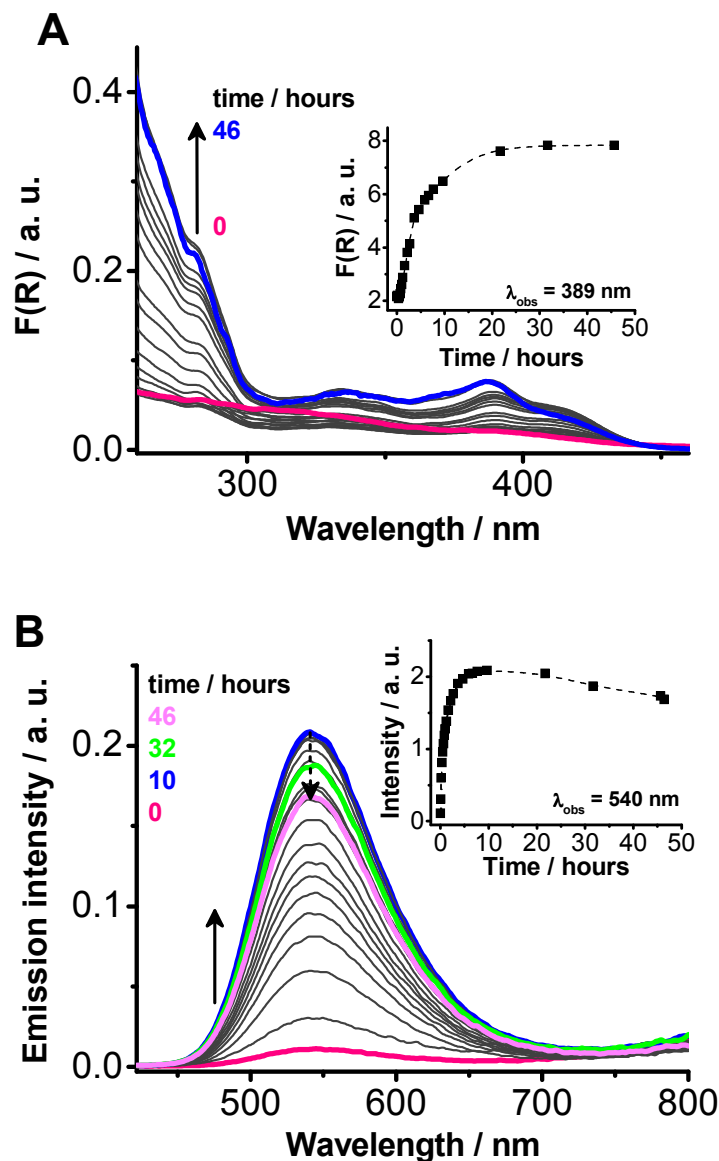

Figure S9. (A) Diffuse reflectance (Kubelka-Munk units) and (B) emission intensity (λ_{exc} = 411 nm) values of 15 days-old **1**-loaded (payload = 33 wt%) nanoMOFs in PBS (pH = 7.4) at different times of incubation. The temperature during the delivery experiments was 29ºC. The concentration of the solution used for the delivery experiment was 0.5 mg nanoMOFs/mL PBS. Insets: variation of the (A) diffuse reflectance (λ_{obs} = 389 nm) and (B) emission intensity (λ_{obs} = 540 nm) values of the 15 days-old **1**-loaded (payload = 33 wt%) nanoMOFs in PBS (pH = 7.4) at 29°C at different times of incubation. The dashed lines are just to guide the eyes.

Clearly, the **1** release is still effective, and it takes over 10 hours. At very long times (> 10 hours), the dimerization of released M to give D is well detectable both in absorption (the ratio A_{389}/A_{418} increases for the formation of D) as in emission (the emission intensity decreases for the fluorescence quenching process occurring at high D concentrations). After ~ 50 hours, the released drug corresponds to about the 20 % of the encapsulated one.
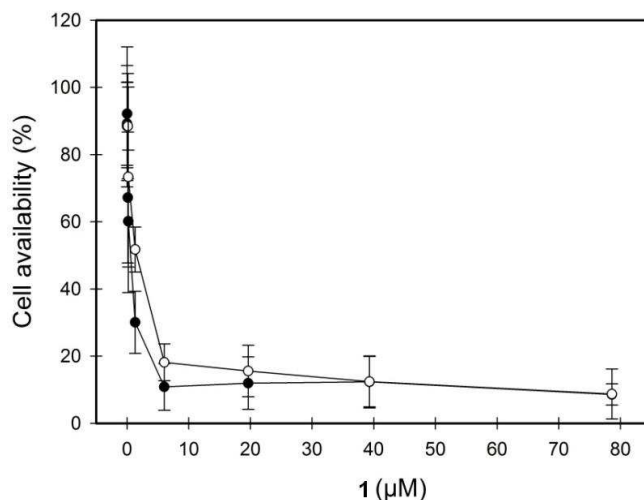
In Vitro Activity of 1-Loaded MIL-100 NanoMOFs
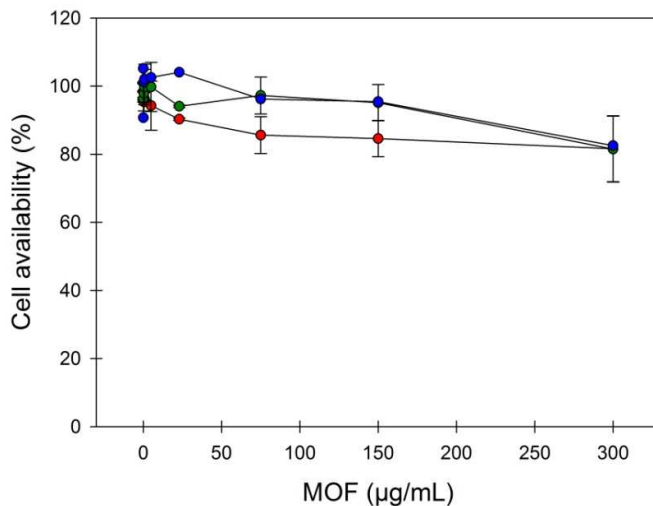
Figure S10. In vitro toxicity of empty MIL-100 nanoMOFs against A549 (blue) MiaPaca2 (green) and PANC1 (red) cell lines measured by MTT assay after 72 h of incubation with increasing nanoparticles concentrations.
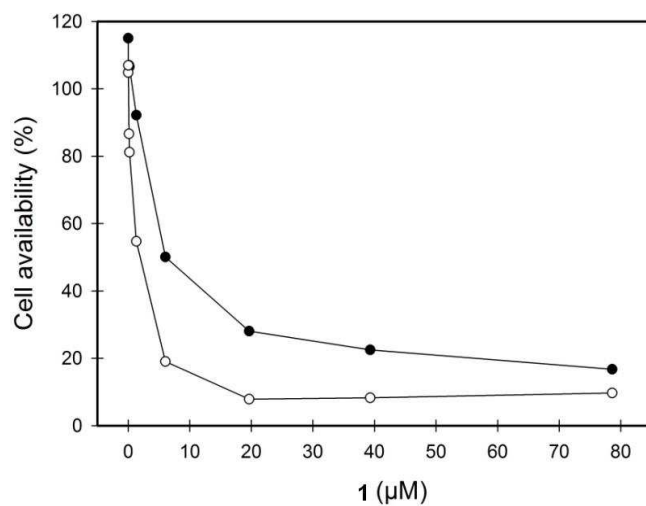
Figure S11. In vitro anti proliferative effect against the human alveolar adenocarcinoma cell line A549 of free **1** (white dots) and **1**-loaded MIL-100 nanoMOFs (black dots) measured by MTT assay after 72 h of incubation with increasing drug concentrations.

Figure S12. In vitro anti proliferative effect against the human pancreatic cancer cell line MiaPaCa2 of free **1** (white dots) and **1**-loaded MIL-100 nanoMOFs (black dots) measured by MTT assay after 72 h of incubation with increasing drug concentrations.

Photon-Induced 1 Release

1 release can also be light-triggered using both one-photon absorption (OPA, λ_{exc} = 390 nm) and two-photon absorption (TPA, λ_{exc} = 780 nm).

Multiphoton processes depend on the near simultaneous ($\sim 10^{-6}$ s) absorption of two (or more) photons both interacting with the molecule, thus resulting in a quadratic dependence on the light intensity rather than the linear dependence in the conventional fluorescence. The attenuation of a beam light resulting from TPA, is given, following the Beer-Lambert's law, by Equation S10:

$$\partial I / \partial z = -N\sigma I^2 \tag{S10}$$

Here, I is the intensity (photons s^{-1} cm^{-2}), z is the distance into the medium, N is the number of molecules per unit volume, and σ (expressed in Göppert-Mayer units, where 1 GM $\equiv 10^{-50}$ cm^4 s photons^{-1} molecule^{-1}). The intensity square dependence is because of the localized nature of the multiphoton event. In order to get elevated instantaneous intensities on a small excitation volume, ultrafast lasers producing ultrashort ($\sim$ 100 fs) pulses at high repetition rates ($\sim$ 80 million pulses per second) are used for non-linear excitation experiments, while continuum wavelength (CW) lasers or non-laser sources are usually employed for conventional spectroscopy. The relative probability of TPA is given by Equation S11:[6]

$$P_2 / P_1 = \sigma_2 I / 2\sigma_1 \tag{S11}$$

In the above equation, $P_1 = \sigma_1 \cdot I$ and $P_2 = \sigma_2 \cdot I^2 / 2$ are the interaction probabilities for one- and two-photon excitation, respectively, where σ_1 and σ_2 are the one- and two-photon cross sections, in that order, and I is the intensity (photons s^{-1} cm^{-2}).

The effect of the photon irradiation on the yield of **1** delivery increases with the drug loading (Figure S13 and S14). In particular, the photoinduced **1** release is 2.25, 2.6, and 500 times higher than the co-respective thermal one for 1.4, 11.6, and 33 wt% **1**-loaded nanoparticles, respectively (Table S5).
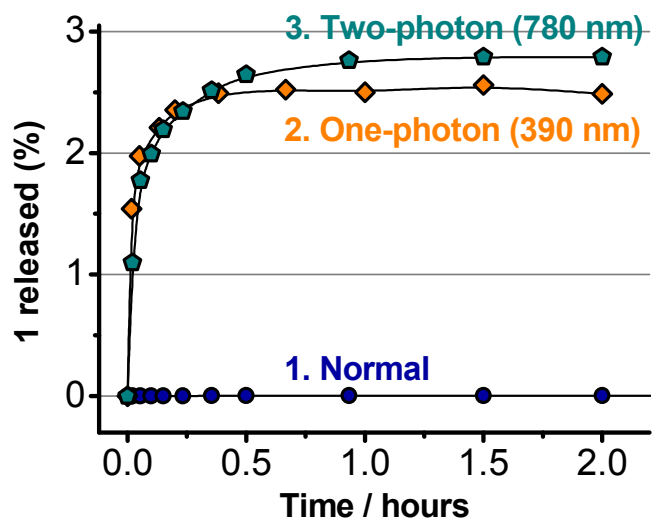
Table S5. Percentages of 1 released from 1-loaded nanoMOFs at different payloads (1.4, 3.5, 11.6, and 33 wt%) and in different media (PBS, pH = 7.4, and water, pH ~ 6.7) in absence and presence of irradiation using one (390 nm, repetition rate = 20 MHz) or two (780 nm, repetition rate = 82 MHz) photons

Payload (wt%)	Normal delivery		Photodelivery one photon (Exc = 390 nm)	Photodelivery two photons (Exc = 780 nm)	
	1 released (%)				
	PBS (pH = 7.4)	water (pH ~ 6.7)	water (pH ~ 6.7)	PBS (pH = 7.4)	water (pH ~ 6.7)
1.4	93	4	9		
3.5	56				
11.6	40	5	13	29	28
33	15	0.005	2.5		2.8

For the highest payload (33 wt%), the percentages of **1** released in water (pH ~ 6.7), being unimportant (0.005%) in absence of light, increase up to 2.5% and 2.8% upon one- and two-photon irradiation, correspondingly. However, taking into account the higher pulse repetition rates used for the TPA deliveries (~ 80 MHz) than those used for the OPA ones (20 MHz), the corrected efficiencies of TPA-release are 6.8% and 0.68% for the payloads 13 and 33wt%, respectively. Despite the use of very high photon densities for TPA-deliveries ($I_{2h\nu}/I_{1h\nu} \sim 1 \times 10^8$), the discrepancy in the yields of **1** photorelease using two photons instead of one is explained on the basis of: 1) the different probabilities of interaction of the molecular ensemble with one or two photon, the latter being ten orders of magnitude lower ($P_2/P_1 = 6.37 \times 10^{-10}$) than the conventional one; 2) a larger laser-excited volume, and, thus, a greater number of excited molecules, in presence of one- than two-photon irradiating light. In particular, we estimated, for our experimental set-up, excitation volumes of ~ 0.4 cm^3 (corresponding to a concentration of ~ 0.2 mg nanoMOFs/mL) and 1.4×10^{-7} cm^3 (corresponding to a concentration of ~ 7×10^{-8} mg nanoMOFs/mL) for OPA and TPA, respectively. For the estimation of the laser-excited sections, *vide infra*.
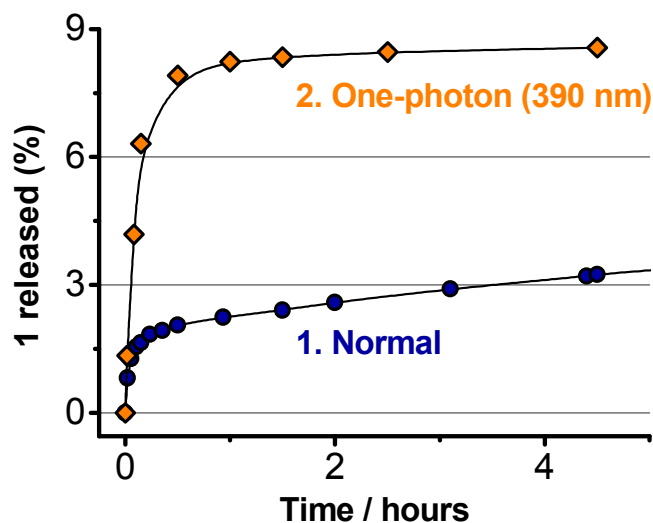
Figure S13. Percentages of **1** released from **1**-loaded (1.4 wt%) nanoMOFs in water at pH ~ 6.7 (1) without and under irradiation with (2) one (λ_{exc} = 390 nm) photon. The release studies were performed at 37°C, and using ~ 0.5 mg nanoMOFs/mL solvent.


Figure S14. Percentages of **1** released from **1**-loaded (33 wt%) nanoMOFs in water at pH ~ 6.7 (1) without and under irradiation with (2) one (λ_{exc} = 390 nm) and (3) two (λ_{exc} = 780 nm) photons. The release studies were performed at 37°C, and using ~ 0.5 mg nanoMOFs/mL solvent.

Estimation of the Laser-Excited Volumes in One- and Two-Photon Excitation Experiments

For one-photon absorption (OPA) experiments, we calculated the irradiated volume as the volume of the cylindrical section of the cell which is passed through the laser beam, as it is shown in Scheme S2:

Scheme S2.
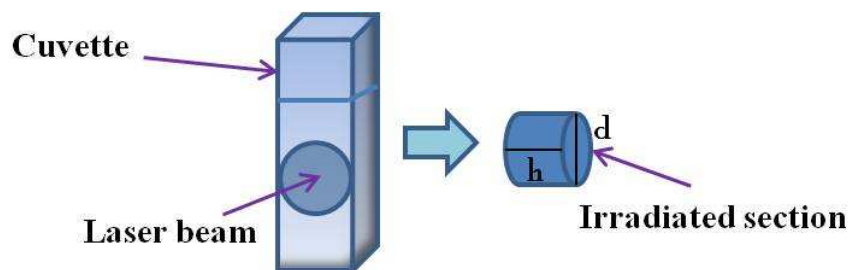
Knowing the diameter of the laser beam (measured d = 0.70 cm) and the optical path-length (1 cm) of the used cell, the irradiated section was thus calculated as:

$$V = \pi \cdot (d/2)^2 \cdot h = 0.38 \ cm^3 \tag{S12}$$

For two-photon absorption (TPA) experiments, we calculated the irradiated volume as the volume of the sphere generated by the high density laser beam in the focal plane. To estimate the diamter of the sphere, we made use of the knife-edge technique.[7] In this technique, a knife edge moves perpendicular to the direction of propagation of the laser beam, and the total transmitted power is measured as a function of the knife-edge position. The knife-edge technique requires a sharp edge, a translation stage with a micrometer, and a power meter or an energy meter when working with pulses.

In our case, we used a thin metallic shutter assembled on a translational stage. Firstly, we measured the laser power. Secondly, we measured two different positions of the knife-edge: 1) the starting one, corresponding to a 15%-reduced laser power; 2) the final one, corresponding to a 85%-reduced laser power. The diameter of the beam was then obtained subtracting the initial position from the starting one like follows:

i.   measured laser power: 2.27 W;

ii.   mm corresponding to a 15%-reduced power (1.93 W) = 3.085;

iii.   mm corresponding to a 85%-reduced laser power (0.34 W) = 3.149;

iv.   diameter = 3.149 mm-3.085 mm = 0.064 mm = 64 μm.

The volume of the sphere was finally calculated as:

$$V = 4/3 \cdot \pi \cdot (d/2)^3 = 1.37 \times 10^{-7} \ cm^3 \tag{S13}$$

All the above measurements were performed always in correspondence of the focal plane.

Calculation of the Laser Intensity in One- and Two-Photon Excitation Experiments

To estimate the intensity from measured laser power readings, we used Equation S14:[8]

$$1 \ mW = \lambda \times 5 \times 10^{12} \ photons \ s^{-1} \ nm^{-1} \tag{S14}$$

This equation is derived from the relationship $E = hc/\lambda$. Equation S14 gives the number of photons per unit time at a given laser power and excitation wavelength. Dividing this value by the area of the beam, we obtained the laser intensity.

For OPA experiments:

Laser power = 500 μW = 500 μJ s^{-1}

λ_{exc} = 390 nm

Beam area = 0.3848 cm^2

1 mW = 1.95 $\times$ 10^{15} photons s^{-1}

500 μW = 9.75 $\times$ 10^{14} photons s^{-1}

$I_{1h\nu}$ = (9.75 $\times$ 10^{14} photons s^{-1})/0.3848 cm^2 = 2.53 $\times$ 10^{15} photons s^{-1} cm^{-2}

For TPA experiments:

Laser power = 2.84 W = 2.84 J s^{-1}

λ_{exc} = 780 nm

Beam area (at the focal plane) = 3.217 $\times$ 10^{-5} cm^2

1 mW = 3.90 $\times$ 10^{15} photons s^{-1}

2.84 W = 1.11 $\times$ 10^{19} photons s^{-1}

$I_{2h\nu}$ = (1.11 $\times$ 10^{19} photons s^{-1})/(3.217 $\times$ 10^{-5} cm^2) = 3.45 $\times$ 10^{23} photons s^{-1} cm^{-2}
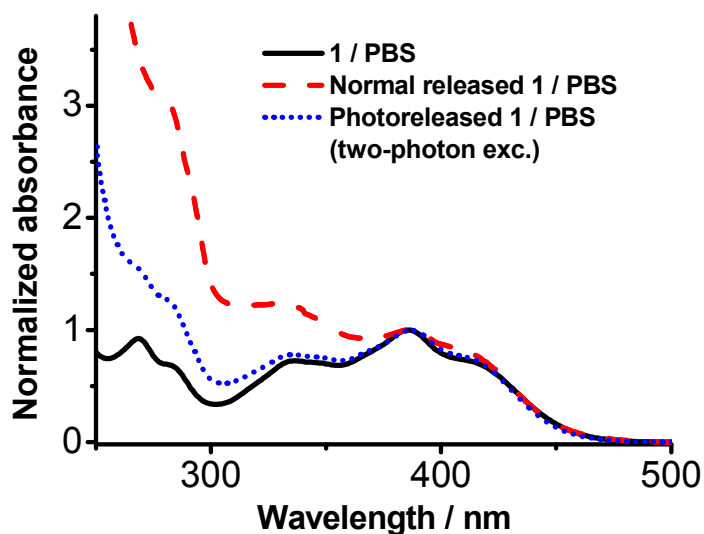

1 Encapsulation within MIL-100 NanoMOFs
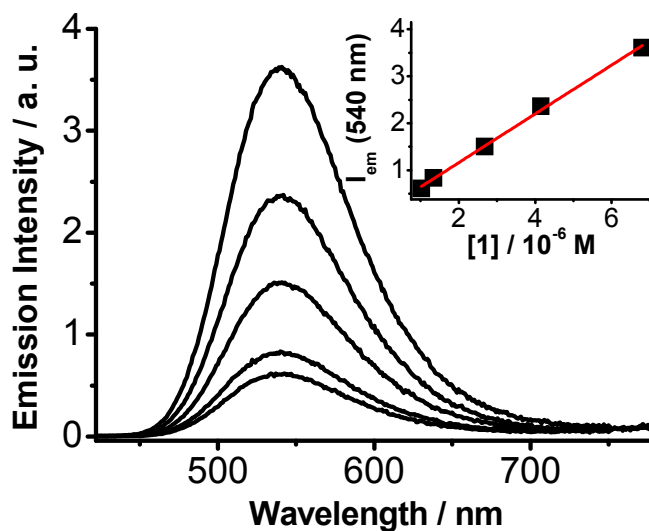
Figure S15. Fluorescence emission spectra of **1** in water at pH $\sim$ 6.7 (λ_{exc} = 411 nm) as a function of concentration (from 1.02 $\times$ 10^{-6} M to 6.80 $\times$ 10^{-6} M). Inset: variation of the intensity of emission of **1**

in water (pH ~ 6.7) at 540 nm with the drug concentration. The red line is the linear fit of the experimental data.

Stability of Released 1

Figure S16. Normalized (to 1) absorption spectra of **1**: 1) 1.42×10^{-4} M in PBS (pH = 7.4, black solid line); 2) after ~ 26 hours of release from **1**-loaded (3.5 wt%) nanoMOFs in PBS at 37ºC (red dashed line); 3) after 2 hours of release from **1**-loaded (11.6 wt%) nanoMOFs in PBS under irradiation with two photons (780 nm, repetition rate = 82 MHz) at 37°C.

Supplementary References

1. Strel'tsov, S. A.; Grokhovskii, S. L.; Kudelina, I. A.; Oleinikov, V. A.; Zhuze, A. L. Interaction of Topotecan, DNA Topoisomerase I Inhibitor, with Double-Stranded Polydeoxyribonucleotides. 1. Topotecan Dimerization in Solution. *Mol. Biol.* **2001**, *35*, 365-373.

2. di Nunzio, M. R.; Wang, Y.; Douhal, A. Structural Spectroscopy and Dynamics of Inter-and Intramolecular H-Bonding Interactions of Topotecan, a Potent Anticancer Drug, in Organic Solvents and in Aqueous Solution. *J. Phys. Chem. B* **2012**, *116*, 7522-7530.

3. López Arbeloa, F.; Ruiz Ojeda, P.; López Arbeloa, I. Dimerization and Trimerization of Rhodamine 6G in Aqueous Solution. *J. Chem. Soc., Faraday Trans. 2* **1988**, *84*(*12*), 1903-1912.
4. Othman, M.; Bouchemal, K.; Couvreur, P.; Gref, R. Microcalorimetric investigation on the formation of supramolecular nanoassemblies of associative polymers loaded with gadolinium chelate derivatives. *Int. J. Pharm.* **2009**, *379*(*2*), 218-225.
5. Segura-Sanchez, F.; Bouchemal, K.; Lebas, G.; Vauthier, C.; Santos-Magalhaes, N. S.; Ponchel, G. Elucidation of the complexation mechanism between (+)-usnic acid and cyclodextrins studied by isothermal titration calorimetry and phase-solubility diagram experiments. *J. Mol. Recognit.* **2009**, *22*(*3*), 232-241.
6. Karotki, A.; Khurana, M.; Lepock, J. R.; Wilson, B. C. Simultaneous Two-photon Excitation of Photofrin in Relation to Photodynamic Therapy. *Photochem. Photobiol.* **2009**, *82*, 443-452.
7. de Araújo, M. A. C.; Silva, R.; de Lima, E.; Pereira, D. P.; deOliveira, P. C. Measurement of Gaussian laser beam radius using the knife-edge technique: improvement on data analysis. *Appl. Opt.* **2009**, *48*(*2*), 393-396.
8. Zipfel, W. R.; Williams, R. M.; Webb, W. W. Nonlinear magic: multiphoton microscopy in the biosciences. *Nat. Biotechnol.* **2003**, *21*(*11*), 1369-77.